

Electronic Supplementary Information for

Shell Effects on Hole-Coupled Electron Transfer Dynamics from CdSe/CdS Quantum Dots to Methyl Viologen

Peng Zeng,^a Nicholas Kirkwood,^{ab} Paul Mulvaney,^{ab} Klaus Boldt,^c and Trevor
A. Smith*^a

a. School of Chemistry, The University of Melbourne, Parkville, Victoria 3010, Australia,

b. Bio21 Institute, The University of Melbourne, Parkville, Victoria 3010, Australia, and

*c. Department of Chemistry & Zukunftskolleg, University of Konstanz, 78457 Konstanz,
Germany*

Corresponding author: Trevor A. Smith

E-mail: trevoras@unimelb.edu.au

TEM Images of CdSe/CdS. Actual shell thicknesses were measured using TEM (200keV Technai TF-20) as shown in Figure S1. They were close to those predicted from shell growth calculations. The CdSe core possesses an average diameter of 4.84 ± 0.28 nm. The average CdS shell thicknesses are 4.1 \AA (1.2 MLs), 12.6 \AA (3.7 MLs) and 19.4 \AA (5.7 MLs), respectively.

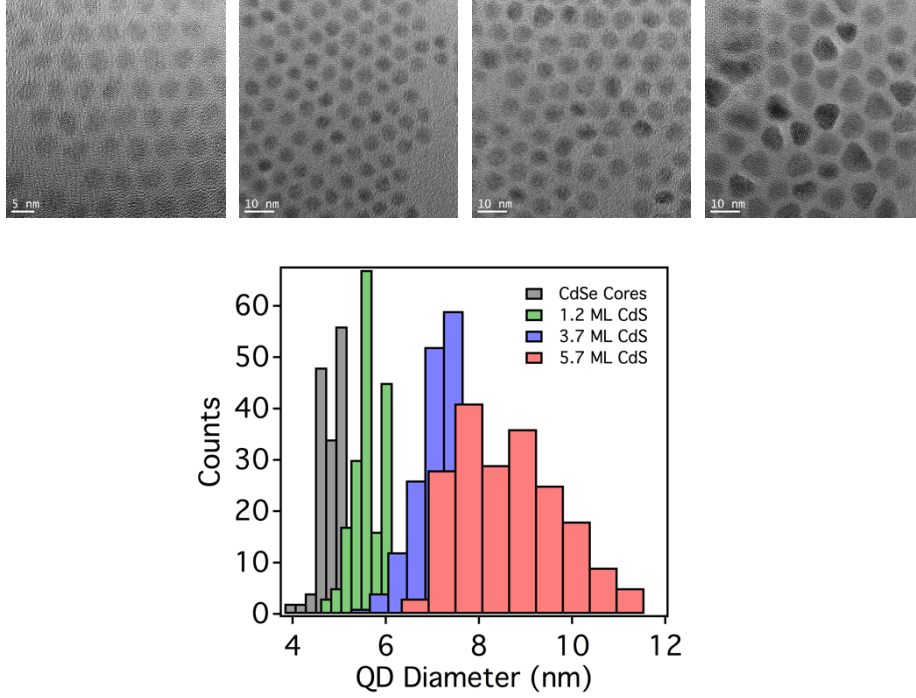


Figure S1. TEM images of CdSe/CdS QDs. The average diameters of the CdSe/CdS QDs core are 4.84 ± 0.28 nm for 0 ML, 5.66 ± 0.36 for 1.2 MLs, 7.30 ± 0.67 for 3.7 MLs, and 8.64 ± 1.07 for 5.7 MLs of the CdS shell (from left to right). The histogram below shows the size distribution of the CdSe/CdS QDs.

The Average Number of Excitons per Particle $\langle N_{\text{ex}} \rangle$. To avoid multi-exciton effects, samples were excited with moderate pulse energies. The average number of excitons per particle, $\langle N_{\text{ex}} \rangle$, should be kept far below 1.

In our study, by knowing the concentrations of samples and absorbance at pump wavelength (400 nm), we gave a simple estimation of $\langle N_{\text{ex}} \rangle$ as follows,

$$\langle N_{\text{ex}} \rangle = \eta \frac{\Phi_{\text{absorb}}}{N_{\text{QD}}} = \eta \frac{\Phi_{\text{incident}} (1 - 10^{-\text{OD}})}{N_{\text{QD}}}, \quad (\text{s1})$$

where N_{QD} is the number of QD particles in the laser path, which can be derived by estimating the illuminated volume in the cuvette (cuvette pathlength ~ 2 mm, laser spot size $\sim 200 \mu\text{m}$ in diameter, and $[\text{QD}] \sim 3 \mu\text{M}$). OD is the absorbance of samples at the excitation wavelength ~ 400 nm, measured by UV-vis absorption spectrometer. Φ_{incident} is the incident excitation laser photon flux. And η is the

photon-exciton transform factor, here we assume $\eta = 1$, indicating an upper limit of $\langle N_{\text{ex}} \rangle$. Table S1 shows the calculated average number of excitons per particle in this study.

Table S1. Calculated average number of excitons per particle, $\langle N_{\text{ex}} \rangle$

	OD@400 nm	Excitation pulse energy /nJ	$\langle N_{\text{ex}} \rangle$
1.2 MLs	0.49	22	0.25
3.7 MLs	1	6.5	0.1
5.7 MLs	3	5.4	0.1

The spot size of the excitation pulse was estimated to be 200 μm in diameter with the knife-edge scanning method. The sample concentrations were about 3 μM . Samples were in a 2 mm-path-length cuvette.

Comparison of Bleaching Kinetics from $1S_e1S_{3/2}$ and $1S_e2S_{3/2}$ State.

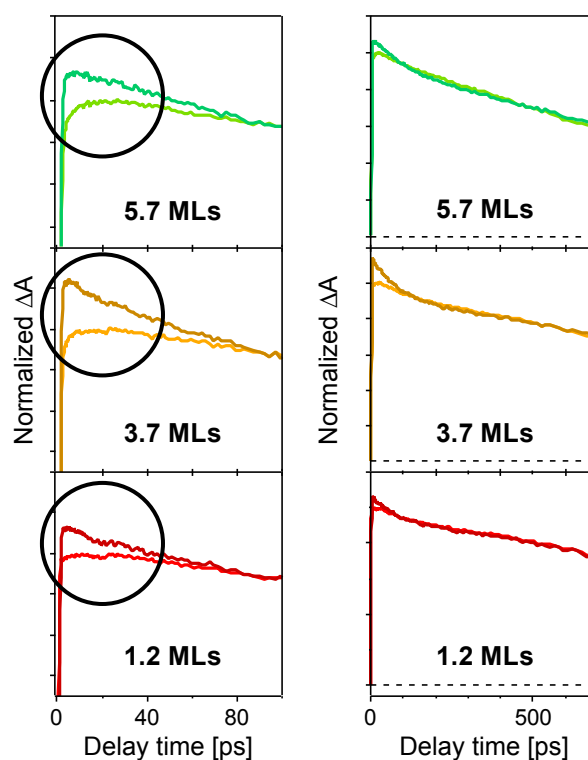


Figure S2. Comparison of normalized $1S_e1S_{3/2}$ and $1S_e2S_{3/2}$ bleaching kinetics in the CdSe/CdS QDs. The $1S_e2S_{3/2}$ signal exhibits a faster decay at short timescales (left circled region), which is attributed to hot hole relaxation from $2S_{3/2}$ to $1S_{3/2}$ with an estimated lifetime of 20–40 ps. The two states show identical kinetics at longer time scales (right).

TA Bleaching Kinetics with Varying Amount of Added MV. We prepared the QD-MV²⁺ complex solution by adding MV²⁺ dissolved in methanol (1 mM) into 600 μ L QD solution step by step after each TA measurement. The molar ratio between added MV²⁺ and QD varied from 0 to 50. The experimental conditions were kept identical at each molar ratio. Figure S2 shows the TA bleaching kinetics of the 1S_e1S_{3/2} state for each QD-MV²⁺ complex. The bleach amplitude becomes smaller and the signals in all three samples exhibit a faster decay with increasing MV²⁺ concentrations, as a result of multiple ET pathways when multiple active MV²⁺ are bound to each QD.

TA Spectral Slices in a range between 600 and 700 nm.

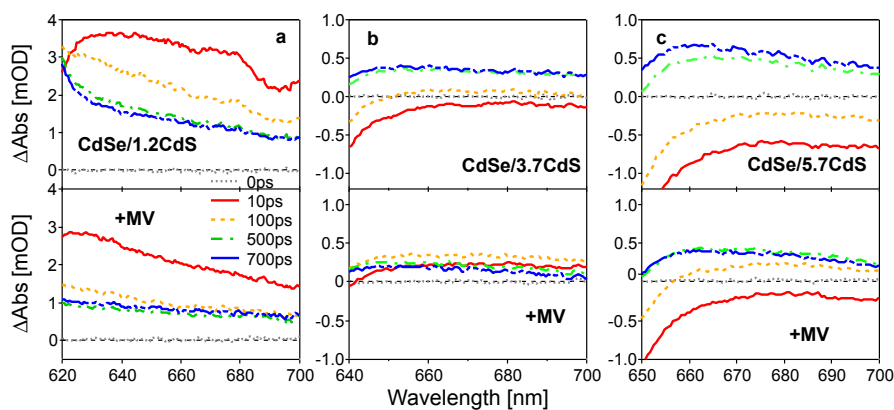


Figure S3. TA slices of QDs and QD-MV complexes at different delay times.

Determination of the Average Number of ET-Active MV²⁺ per QD, λ . Based on Weiss's method [1], we determined λ by an analysis of the TA bleaching amplitude. It is assumed that: (a) any QD with one or more active MV²⁺ will undergo an ET process, thus the bleach will recover due to the transfer of electrons; (b) the kinetics at long delay times are independent of the ET process since ET occurs on fast time scales. Therefore the ratio of the amplitude of the bleach signal in a sample of QDs with MV²⁺, B , to that in a sample with only QDs, B_0 , is the fraction of QDs without ET-active MV²⁺ in the sample, given by

$$f(0) = \frac{B}{B_0}. \quad (\text{s2})$$

Assuming a Poisson distribution of QD-MV²⁺ particles [2, 3], the fraction of QDs with n ET-active MV²⁺ is:

$$f(n) = \frac{\lambda^n e^{-\lambda}}{n!}. \quad (\text{s3})$$

where λ is the mean number of MV^{2+} ions per QD. By combining the two equations above, we obtain the value of λ when $n = 0$:

$$\lambda = -\ln(B/B_0). \quad (\text{s4})$$

In order to obtain B and B_0 , we integrated the bleach amplitudes in time windows at relatively long time scale, 300-400 ps for CdSe/1.2CdS, 300-400 ps for CdSe/3.7CdS and 500-700 ps for CdSe/5.7CdS, as shown in Figure S4. These time windows were selected by noting that the ET process should be complete before the selected time window and a good S/N ratio is required within the time window. The intrinsic ET time constants were calculated to be 40 ps, 45 ps and 244 ps for CdSe/1.2CdS, CdSe/3.7CdS and CdSe/5.7CdS, respectively, indicating the ET processes were almost complete before the time windows we selected. Also, the bleaching kinetics within the selected time windows show similar trends in each batch of QDs for different concentrations of added MV^{2+} . This is consistent with our assumption that the kinetics at long delay times is independent of the ET process.

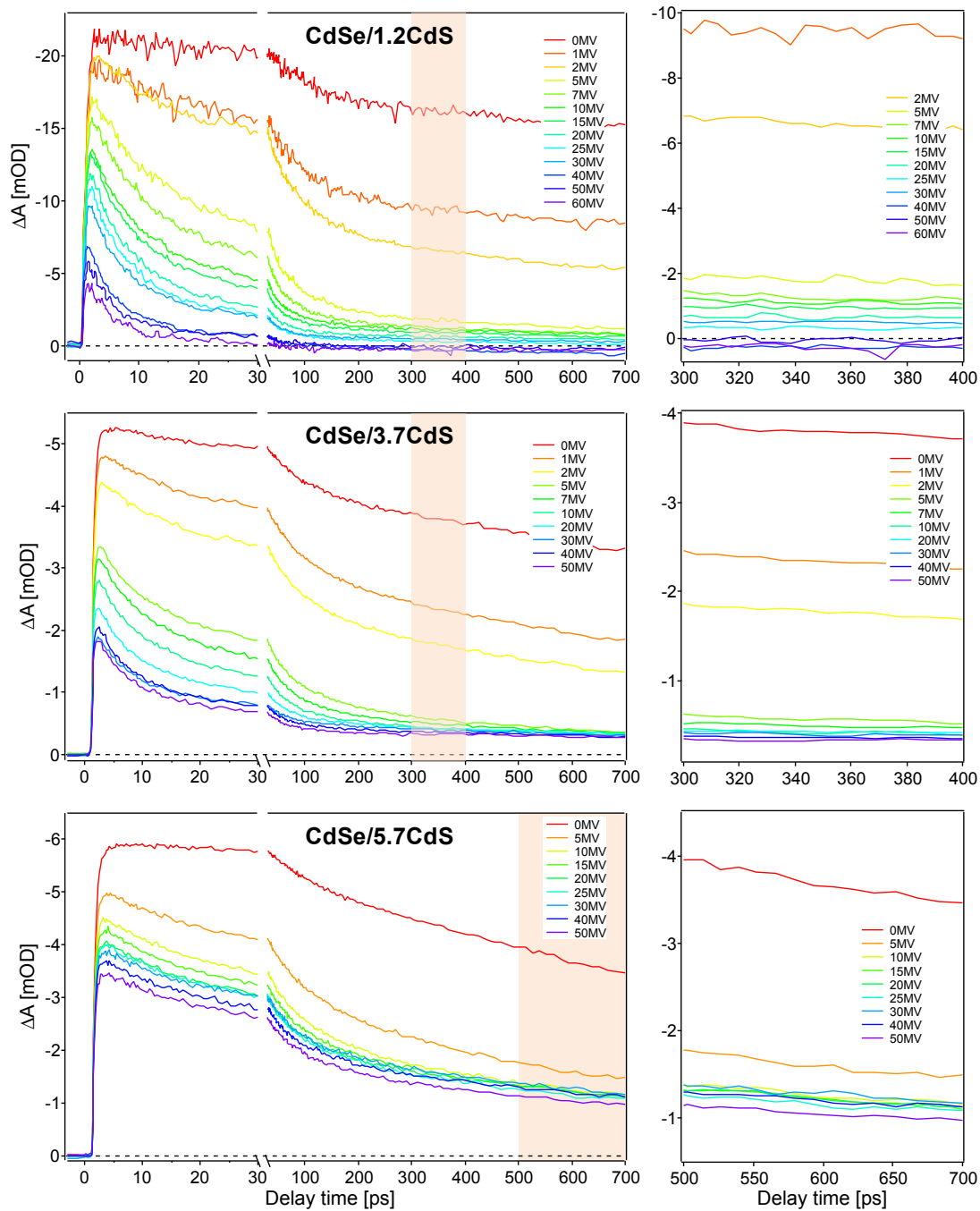


Figure S4. The TA bleaching kinetics probed at $1S_e1S_{3/2}$ in QD- MV^{2+} complexes, as a function of the concentration of added MV^{2+} . The laser conditions were kept identical for every TA measurement on a given batch of QDs. Plots on the right side show higher resolution images of part of the selected time windows (shaded areas in the left figures) for calculation of λ .

The Average Number of ET-Active MV^{2+} per QD, λ , as a Function of Concentration of Free MV^{2+} . A Langmuir isotherm model was applied to fit the values for λ determined in the previous section as a function of the concentration of free MV^{2+} in the solution. The fitting function is given as

$$\lambda = \lambda_{\max} \frac{K_a [\text{MV}^{2+}]_{\text{free}}}{1 + K_a [\text{MV}^{2+}]_{\text{free}}}, \quad (\text{s5})$$

where $[\text{MV}^{2+}]_{\text{free}}$ is the concentration of free MV^{2+} in the QD- MV^{2+} complex solution and was determined using the previously calculated value for λ , the total concentration $[\text{MV}^{2+}]_0$ and the QD concentration $[\text{QD}]$.

$$\begin{aligned} [\text{MV}^{2+}]_{\text{free}} &= [\text{MV}^{2+}]_0 - [\text{MV}^{2+}]_{\text{adsorbed}}, \\ &= [\text{MV}^{2+}]_0 - \lambda \cdot [\text{QD}] \end{aligned}, \quad (\text{s6})$$

K_a is the adsorption constant, which is sensitive to absolute values of concentrations. λ_{\max} is the maximum number of available surface binding sites per QD for MV^{2+} . The function is plotted in Figure 5. Weiss et al. studied the concentration dependence for the adsorption of ligands onto QDs [4]. They reported a smaller fractional surface coverage of electron acceptors on the QD in QD-ligand solutions with higher QD concentration, which they interpreted in terms of aggregation of QD clusters with high concentration. In our study, however, the investigated QD- MV^{2+} solutions have identical concentrations but with different QD sizes, indicating that the observed dependence of λ_{\max} is related to QD size rather than aggregation effects.

Calculation of the Intrinsic ET Rate k_{ET} . The calculation and analysis methods are based on Weiss's [1] and Lian's [5] work. The TA bleaching decay can be fit with an infinite sum $g(t)$ of exponential components $A_i \exp(-k_i t)$, given as

$$N(t) = N(0) \cdot g(t) = N(0) \sum_i A_i e^{-k_i t}. \quad (\text{s7})$$

For QV- MV^{2+} complexes, electrons have an additional transfer way to adsorbed MV^{2+} with a rate k_n

$$k_n = nk_{ET}. \quad (\text{s8})$$

Thus we have the decay kinetics involving the ET process based on a linear assumption, and the intrinsic ET rate k_{ET} is derived as

$$k_{ET} = -\frac{1}{\tau_{1/2}} \ln \left[1 - \frac{\ln(2g(\tau_{1/2}))}{\lambda} \right], \quad (\text{s9})$$

by following Lian's work [5], where $\tau_{1/2}$ is the measured duration for the maximum bleaching intensity to halve in QD-MV²⁺ complexes. $g(t)$ is the measured bleaching decay in QDs without MV²⁺.

Calculation of Electron and Hole Wavefunction. The electron and hole wave functions have been determined using Mathematica by numerically calculating the radial eigenfunctions of spherical core/shell QDs, forming a two-step potential well [7,8]. The parameters used are summarized in Table S2. A CdSe core radius of 2.4 nm and between 1 and 5 monolayers of CdS with a thickness of 3.38 Å per monolayer were employed. Coulomb attraction was treated as a perturbation to determine the energy eigenvalues.

Table S2. Parameters used for the calculation of charge carrier eigenfunctions.

Material	$m_e^* [m_e]$	$m_h^* [m_e]$	ϵ_r	U_{CB} [eV]	U_{VB} [eV]
CdSe	0.11	0.44	10.00	-3.96	-5.7
CdS	0.18	0.60	5.40	-3.84	-6.30
Matrix	1	1	1	0	-10

According to Zhu et al. [6] the electron transfer rate can be extracted from Marcus theory:

$$k_{ET}(d) = \frac{2\pi}{\hbar} \frac{|H(d)|^2}{\sqrt{4\pi\lambda_E k_B T}} \exp\left(-\frac{(\lambda_E + \Delta G(d))^2}{4\lambda_E k_B T}\right) \quad (s10)$$

The electronic coupling strength $H(d) = \langle \Psi_{MV} | \hat{H} | \Psi_e \rangle$ is the matrix element for the transition of the 1S electron from the QD to the LUMO of MV²⁺. The transfer rate should therefore be proportional to the coupling strength at the particle surface.

$$k_{ET} \propto |\Psi(R_{\text{surface}})|^2 \quad (s11)$$

From these assumptions we extracted the coupling strengths summarized in Table S3. Figure S6 shows an exponential fitting to the scaled $|\Psi(R)|^2$, giving an attenuation factor β of $(0.18 \pm 0.01) \text{ \AA}^{-1}$ (Error indicates the 95% confidence interval of the fitting parameter given by the fitting method.).

Table S3. Calculated coupling strengths for 1–5 monolayers of CdS.

Monolayer	1	2	3	4	5
Thickness [Å]	3.4	6.8	10.2	13.6	17.0
$\Psi(R_{\text{surface}}) ^2$	0.0308	0.0149	0.0078	0.0044	0.0026

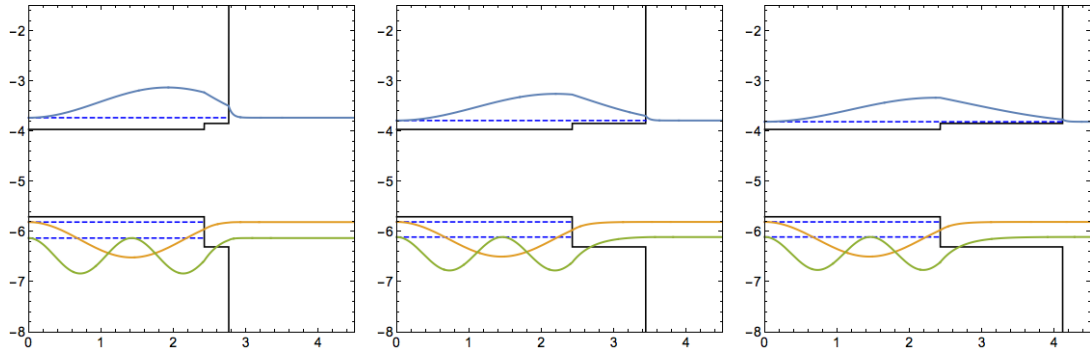


Figure S5. Plots for the radial probability of position $|\Psi(R)|^2R^2$ of the calculated 1S electron (blue), 1S_{3/2} hole (yellow) and 2S_{3/2} hole (green) for 1, 3, and 5 monolayers of CdS from left to right.

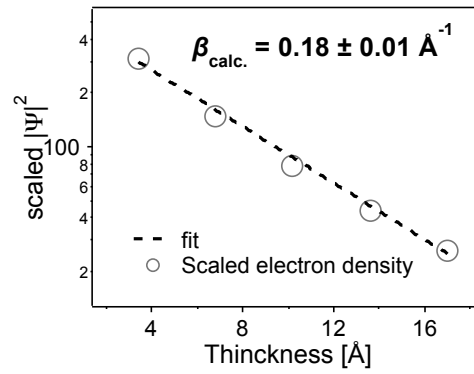


Figure S6. Fitting of the scaled $|\Psi(R)|^2$.

TCSPC measurement of PL decay kinetics. Figure S7 shows PL decay kinetics of CdSe/CdS QDs in the absence and presence of MV²⁺. Excitation was at 400 nm with a pulse width of 100 fs. Instrument response function (IRF) was also measured and shown in Figure S7 (a). A multi-exponential function convoluted with IRF was fit to the measured data as indicated by black lines. Fitting results are summarized in Table S4.

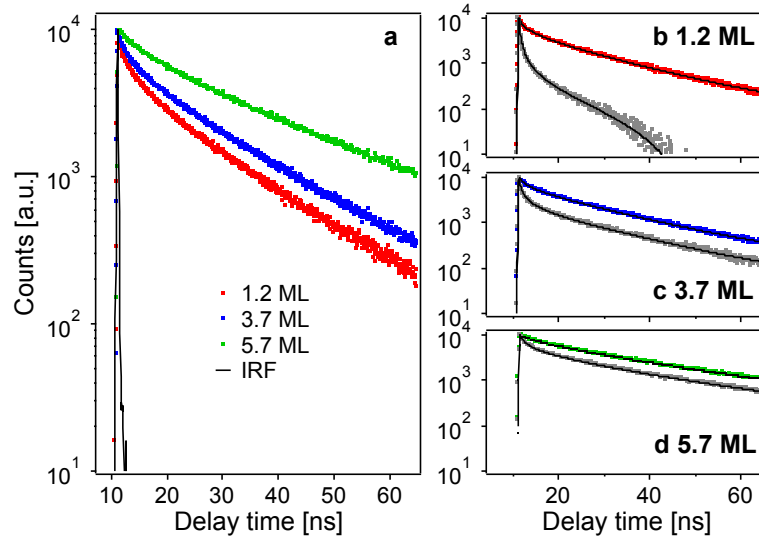


Figure S7. TCSPC results. (a) A comparison of PL decay curves from CdSe/CdS QDs. Excitation was at 400 nm with a pulse width of 100 fs. The concentrations were around 70 nM. IRF was also measured and indicated by black line in (a). (b)-(d) Comparisons and multiexponential fittings of PL decays of CdSe/CdS QDs in the absence and presence (gray dots) of MV^{2+} . PL decays faster in QD- MV^{2+} complexes. The added $MV:QD$ ratio was about 20:1 to all samples.

Table S4. Fitting results of TCSPC measurements of PL decay kinetics.

Sample	$\tau_1 (A_1)$	$\tau_2 (A_2)$	$\tau_1 (A_1)$	$\tau_1 (A_1)$
CdSe/1.2CdS	350ps (33%)	1.5ns (10%)	4ns (36%)	>10ns (3%)
+MV^{2+}	100ps (69%)	600ps (21%)	2.4ns (6%)	>10ns (4%)
CdSe/3.7CdS	650ps (24%)	3ns (22%)	-	>10ns (54%)
+MV^{2+}	200ps (52%)	2ns (31%)	-	>10ns (17%)
CdSe/5.7CdS	2.2ns (15%)	5.3ns (4%)	-	>10ns (81%)
+MV^{2+}	900ps (35%)	4ns (17%)	-	>10ns (48%)

The PL lifetime increases with the CdS shell thickness due to the delocalization of electrons into shells. By comparing lifetime from QDs with and without MV^{2+} , we found that PL decays faster. Time constants of fast components (τ_1) drop to 100-900 ps, while their amplitudes (A_1) increase remarkably in QD- MV^{2+} complexes (τ_1), which we attribute to the ET process. It is consistent with the ET rate we obtained from TA measurement (~ 100 ps).

Reference

- [1] Morris-Cohen, A. J., Frederick, M. T., Cass, L. C., & Weiss, E. A. (2011). Simultaneous Determination of the Adsorption Constant and the Photoinduced Electron Transfer Rate for a Cds Quantum Dot–Viologen Complex. *Journal of the American Chemical Society*, 133(26), 10146–10154. doi:10.1021/ja2010237
- [2] Tachiya, M. (1975). Application of a generating function to reaction kinetics in micelles. Kinetics of quenching of luminescent probes in micelles. *Chemical Physics Letters*, 33(39), 289 – 292.
- [3] Sadhu, S., Tachiya, M. and Patra, A. (2009). A Stochastic Model for Energy Transfer from CdS Quantum Dots/Rods (Donors) to Nile Red Dye (Acceptors). *The Journal of Physical Chemistry C*, 113, 19488–19492.
- [4] Morris-Cohen, A. J., Vasilenko, V., Amin, V. A., Reuter, M. G., & Weiss, E. A. (2012). Model for Adsorption of Ligands to Colloidal Quantum Dots with Concentration-Dependent Surface Structure. *ACS Nano*, 6(1), 557–565. doi:10.1021/nn203950s
- [5] Zhu, H., Yang, Y., Hyeon-Deuk, K., Califano, M., Song, N., Wang, Y., et al. (2014). Auger-Assisted Electron Transfer from Photoexcited Semiconductor Quantum Dots. *Nano Letters*, 14(3), 1263–1269. doi:10.1021/nl4041687
- [6] Zhu, H., Song, N., & Lian, T. (2010). Controlling Charge Separation and Recombination Rates in CdSe/ZnS Type I Core–Shell Quantum Dots by Shell Thicknesses. *Journal of the American Chemical Society*, 132(42), 15038–15045. doi:10.1021/ja106710m
- [7] Schooss, D., Mews, A., Eychmüller, A., & Weller, H. (1994). Quantum-Dot Quantum Well CdS/HgS/CdS: Theory and Experiment. *Physical Review B*, 49(24), 17072–17078.
- [8] Boldt, K., Ramanan, C., Chanaewa, A., Werheid, M., & Eychmüller, A. (2015). Controlling Charge Carrier Overlap in Type-II ZnSe/ZnS/CdS Core-Barrier-Shell Quantum Dots. *The Journal of Physical Chemistry Letters*, 6, 2590–2597. doi:10.1021/acs.jpcllett.5b01144